Applied Catalysis B: Environmental 241 (2019) 483–490

Contents lists available at ScienceDirect

Applied Catalysis B: Environmental

journal homepage: www.elsevier.com/locate/apcatb

In-situ hydrogenation engineering of $ZnIn_2S_4$ for promoted visible-light water splitting

Yanwei Zhu[a], Longlu Wang[a,b], Yutang Liu[c], Luhua Shao[a], Xinnian Xia[a,*]

[a] College of Chemistry and Chemical Engineering, Hunan University, Lushan South Road, Yuelu District, Changsha 410082, PR China
[b] State Key Laboratory of Chemo/Biosensing and Chemometrics, Hunan University, Lushan South Road, Yuelu District, Changsha 410082, PR China
[c] Key Laboratory of Environmental Biology and Pollution Control (Hunan University), Ministry of Education, Lushan South Road, Yuelu District, Changsha 410082, PR China

ARTICLE INFO

Keywords:
In-situ hydrogenation
$ZnIn_2S_4$
Photocatalysis
Hydrogen production

ABSTRACT

Hydrogenation engineering has been considered as one of the promising methodologies to significantly enhance the visible light absorption and photocatalytic activities of semiconductor photocatalyst. However, hydrogenated catalyst with remarkably elevated photocatalytic activity has been commonly obtained so far under severe conditions such as high temperatures or pressures and huge doses of H_2 or plasma activation with complex treatment. Here, we proposed in-situ hydrogenated $ZnIn_2S_4$ (H_xZIS) obtained at room temperature under UV–vis light illumination within several hours. This extremely facile hydrogenation strategy is based on the discovered fact that H could spontaneously adsorb on the $ZnIn_2S_4$ (ZIS) surface to generate durable point defects and even surface disorder, resulting in the largely enhanced solar energy utilization of ZIS. As a result, the hydrogenation engineered the band gap from 2.42 to 1.51 eV, while the optimal bandgap was tuned to ca. 2.08 eV with a ~10-fold photocatalytic activity promotion. This study is the first paradigm of in-situ hydrogenation of inorganic metal chalcogenide, and we believe that such a facile and general methodology will open up a new pathway to create high-efficiency photocatalyst.

1. Introduction

Because of increasing environmental awareness and excessive non-renewable power consumption, the conversion of solar energy into chemical energy via semiconductor photocatalysts has attracted extensive attention, particularly with regard to the utilization of hydrogen energy [1–5]. Yet, to date, the overall photoconversion efficiency is still very low and requires further promotion for commercialization [6,7]. Recently, accompanied by the booming development of graphene and its derivatives, much attention was paid to ultrathin nanosheets of inorganic graphene analogues (IGA) with large specific surface area [8–12]. Among the various inorganic graphene analogues, the layered transition-metal chalcogenides garnered great research interest [13]. ZIS is a ternary chalcogenide with a bandgap of ca. 2.42 eV and has attracted increasing attention largely due to its easy availability, ability of absobing visible light, low-cost, and good stability [14,15]. Concerning the full ultilization of the visible light, the ideal bandgap of a photocatalyst is considered to be ca. 2 eV [16]. Hence, great efforts have been devoted to narrowing the band gap of ZIS and extending its light absorption spectrum to the visible light region, which has mainly involved non-metal doping, noble metal coupling and surface sensitization [17–19]. Recently, a breakthrough on the hydrogenation of TiO_2, giving rise to absorption across the entire visible-light region and remarkable photocatalytic activity under sunlight, has been achieved and has subsequently triggered great research interest worldwide [20,21]. Hydrogenation engineering has been considered as one of the promising methodologies to improve solar energy utilization [20].

Different strategies have been explored to obtain hydrogenated catalysts. The hydrogenation of TiO_2 nanoparticles under 20.0 bar pure H_2 gas pressure at 200 °C for 5 days resulted in extended optical absorption to the near infrared region, and substantially improved the photocatalytic activity with prolonged stability as reported by Chen et al. [22]. Hu et al. reported hydrogenated Cu_2WS_4 as supercapacitors by a lithium intercalation assisted exfoliation strategy, revealing a transition from semiconductor to metal, that is, its conductive nature can be strongly modified by hydrogenation [23]. Other reported methods include hydrogen plasma treatments or hydrogen-argon treatments at 400–700 °C for several to tens of hours [24,25]. Apparently, all these available hydrogenation strategies suffer from especially severe conditions such as high pressure (20.0 bar) and/or high

* Corresponding author.
E-mail address: xnxia@hnu.edu.cn (X. Xia).

https://doi.org/10.1016/j.apcatb.2018.09.062
Received 9 July 2018; Received in revised form 1 September 2018; Accepted 19 September 2018
Available online 22 September 2018
0926-3373/ © 2018 Elsevier B.V. All rights reserved.

temperature (up to 700 °C) over a long period of treatment (up to several days), and dangerous lithium intercalation. It is a big challenge to develop an especially facile and efficient strategy for efficient hydrogenation. Recently, Xu et al. reported a Pd-catalyzed hydrogenation strategy, when incorporating a small amount Pd in rutile TiO_2 for administrating photocatalytic hydrogen evolution, TiO_2/Pd was irreversibly reduced during the photocatalytic water reduction process [20]. This suggests possibly facile and efficient hydrogenation can be achieved by hydrogen atoms in-situ generated during the photocatalytic process directly.

In this work, ZIS was used as photocatalyst for photocatalytic hydrogen evolution reaction (PHER) with an on-line gas chromatography. It was found that the photocatalyst experienced a significant color change from yellow to black in several hours when illuminated by UV–vis light for administrating photocatalytic hydrogen evolution. The photocatalytic hydrogen evolution properties could be adjusted by optimize the amounts of adsorbed H on the surface of ZIS that could be easily realized via vigorous stirring. The optimized ZIS with appropriate adsorbed H exhibits the best photocatalytic performance during the test with a ten-fold H_2 production enhancement compared to pristine ZIS nanosheets. Judging from the ^{1}H solid-state NMR spectroscopy, the two peaks at 3.35 and 4.0 ppm correspond to S—H bonds, giving direct evidence that ZIS had been hydrogenated during the photocatalytic water reduction process, which is further demonstrated by the XPS results [23]. As such, our DFT results suggest that the hydrogen incorporation on the ZIS surface facilitates easier electron excitation and allows for higher carrier density as well as efficient carrier transport along the two-dimensional (2D) conducting channels. These results hold promise for applications of other novel functional materials designing by a self-optimization strategy.

2. Experimental section

2.1. Materials

$Zn(Ac)_2{\cdot}2H_2O$, $InCl_3{\cdot}4H_2O$, thioacetamide (TAA), triethanolamine, lactic acid, $Na_2S{\cdot}9H_2O$, Na_2SO_3, CdS, ZnS were all obtained from Sinopharm Chemical Reagent Co. Ltd and used without further purification. The DI water used in the catalyst preparation was from local sources.

2.2. Preparation of HxZIS and BCHZIS nanosheets

ZIS nanosheets were fabricated by a facile low-temperature refluxing method followed by a moderate exfoliation. In detail, 1.5 mmol of $Zn(CH_3COO)_2{\cdot}2H_2O$ and 3 mmol of $InCl_3{\cdot}4H_2O$ were added into 250 ml DI water and stirred for 1 h. Subsequently, an excess amount of thioacetamide (TAA, 8.5 mmol) was added into the above solution and stirred for another 1 h. The solution was then heated to 95 °C and maintained at that temperature for 8 h under vigorous stirring. The resulted precipitation was collected by centrifugation, rinsed with water for 4 times and re-dispersed into 300 mL DI water. The dispersion was sonicated continuously for 2 h and then centrifuged at 4000 r.p.m. for 10 min to remove aggregates. After that, the colloidal ZIS nanosheets were illuminated under UV–vis light in a 100 mL sealed quartz flask at ambient temperature and atmospheric pressure. Samples obtained with illumination time of 2 h, 4 h, 6 h were denoted as H_xZIS-2 h, H_xZIS-4 h, H_xZIS-6 h, respectively. Sample BCHZIS was obtained via vigorous stirring (1000 r/min, 12 h) under dark after 9-hour illumination.

2.3. Physical characterization

The morphologies and microstructures of the samples were characterized using an S-4800 field emission scanning electron microscope (FESEM, Hitachi, Japan) and a transmission electron microscope (TEM, JEOL JEM-2100F). The EDS mapping images were captured on a Tecnai G2 F20 S-TWIN atomic resolution analytical microscope. The crystal phases of the samples were collected on an X-ray diffractometer with Cu-Kα radiation (XRD, M21X, MACScience Ltd., Japan). Raman microspectrometer (Renishaw, Great Britain) in the range of 500–2100 cm^{-1} under a 785 nm diode laser excitation was carried out. The spectra were collected in a backscattering geometry using a microscope equipped with a Leica 20× objective in a spectral resolution of 2 cm^{-1}. The detection of the Raman signal was carried out with a Peltier cooled charge-coupled device (CCD) camera. The software package WIRE 2.0 (Renishaw) was employed for acquisition and analysis. The UV–vis diffuse reflectance spectra (DRS) were performed on a UV–vis spectrophotometer (Cary 300, USA) with an integrating sphere. BaSO4 was used as a reflectance standard. The photoluminescence (PL) spectra for solid samples were investigated through F-7000. All of the binding energies were referred to the C 1s peak at 284.8 eV of the surface adventitious carbon. 1H solid-state MAS NMR spectra were obtained with a 500.132 MHz NMR spectrometer (Bruker, Germany) at 298 K.

2.4. Electrochemical measurements

The electrochemical impedance spectroscopy (EIS) experiments were carried out with a CHI 660C electrochemical analyzer (CHI Inc., USA) in a three-electrode configuration. FTO electrodes deposited with the samples as anode, a platinum wire as the counter electrode, and a saturated calomel electrode (SCE) as the reference electrode. All the samples were analyzed under room temperature without bias potential. 0.35 M/0.25 M Na_2S-Na_2SO_3 aqueous solution was used as the electrolyte. For the fabrication of the anode, 0.25 g of the sample was grinded with 0.06 g polyethylene glycol (PEG, molecular weight: 20,000) and 0.5 ml ethanol to make a slurry. Then, the slurry was coated onto a 1 cm × 4 cm F-doped SnO_2-coated glass (FTO glass) electrode by the doctor blade technique, and then allowed to dry in air.

2.5. Photocatalytic hydrogen production tests

The photocatalytic hydrogen evolution experiments were performed in a 100 mL sealed quartz flask at ambient temperature and atmospheric pressure. A 300 W xenon arc lamp with lighting wavelength range of 320–780 nm (Perfectlight, PLS-SXE 300C, Beijing, China) was used as light source to trigger the photocatalytic reaction. The lamp was positioned 10 cm away from the reactor where the focused intensity on the flask was 160 mW cm^{-2}. In a typical photocatalytic experiment, 80 mg of photocatalyst was dispersed in an 80 mL mixed aqueous solution containing 0.35 M Na_2S and 0.25 M Na_2SO_3 (pH 13.2). Before irradiation, the system was bubbled with nitrogen for 30 min to remove the air ensuring the reaction system in an inertial condition. The hydrogen was analyzed by gas chromatography (Shimazu GC2010) equipped with a thermal conductive detector (TCD) and a 5 Å molecular sieve column, using nitrogen as the carrier gas.

2.6. DFT calculations

Structural models are represented using the visualization tool Visualization for Electronic and Structural Analysis (VESTA).

3. Result and discussion

3.1. Synthesis of HxZIS and hydrogenation process

The ZIS nanosheets were prepared via a facile low-temperature refluxing method, followed by a water-assisted surfactant/intercalator-free exfoliation process [26]. The morphology of the as-prepared products was observed using SEM (Fig. 1a and b). The SEM images show that the samples possessed large-scale 2D sheet-like structures and the size of these nanosheets were about 1.0 μm and exhibited a well

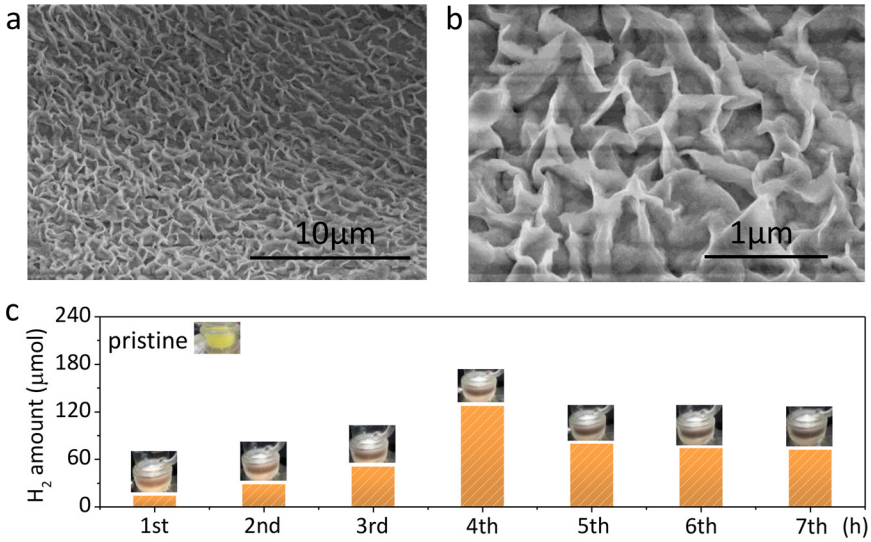

Fig. 1. (a, b) SEM images of ZIS nanosheets. (c) Hydrogen amount and the corresponding color change of the ZIS nanosheets. (For interpretation of the references to colour in the text, the reader is referred to the web version of this article.)

uniformed morphology. TEM image of ZIS nanosheets shown in Fig. S1 indicates the low crystallinity of the product.

Then the as obtained ZIS nanosheets were treated under UV–vis light in sealed quartz flask with Na_2S/Na_2SO_3 as sacrificial agent. Intriguingly, the H_2 evolution rate gradually increases with prolonged illumination time in the first four hours (Fig. 1c). Moreover, the color of ZIS changed gradually from yellow to black in few hours (Fig. 1c). Similar phenomena were also observed in controlled experiment when using methanol and triethanolamine as the sacrificial agent (Figs. S2 and S3). These results indicate that the HER performance of the ZIS nanosheets were being optimized in the first four hours during the illumination. Interestingly, vigorous stirring can bleach its color within 12 h in the dark. Notably, the phenomenon that the activity increased with prolonged reaction time is quite different from the usual metal sulfides, which generally show a decline in activity during the photocatalytic reaction [27–29]. The photocatalytic hydrogen evolution of CdS and ZnS were performed under the same conditions as $ZnIn_2S_4$ (Fig. S4). Similar photocatalytic hydrogen evolution phenomena were also observed in other studies of the HERs over ZIS but the color change was not mentioned [30]. So, it is significant to elucidate the mechanism underlying the color change and accelerated photocatalytic activity of ZIS nanosheets in the first four hours.

^{1}H solid-state NMR spectroscopy was employed to examine the possible generation of H—S bonds, which can provide direct proof for the hydrogenation of ZIS nanosheets. As displayed in the ^{1}HNMR spectra (Fig. 2a), there are four peaks at 0.5, 1.5, 3.35, and 4.0 ppm for the illuminated nanosheets, named as δ_1, δ_2, δ_3 and δ_4, respectively. The two peaks at 3.35 and 4.0 ppm correspond to S—H bonds, giving direct evidence for the presence of hydrogen doping in the illuminated nanosheets. The amounts of doped H gradually increased with the hydrogenation process (Fig. S5). From the chemical states of S 2p (Fig. 2b), there are two types of sulfur in the illuminated nanosheets (pristine and hydrogenated), in accordance with two S—H bonds signals shown in ^{1}HNMR spectra, further confirming that parts of sulfur in ZIS structure were hydrogenated during illumination [23].

3.2. Characterization of HxZIS

H_xZIS samples appear in different colors ranging from cyan to black, in marked contrast to the yellow pristine ZIS powders. Diffuse reflectance ultraviolet-visible (UV–vis) spectroscopy was then employed to investigate the intrinsic optical properties of the pristine and illuminated samples (Fig. 3a). Noticeably, all the samples show fairly high absorbance in the UV and blue region (< 400 nm). ZIS samples absorb most of the UV-blue light and therefore appear yellow in color. For the UV–vis light treated samples, the absorbance in the wavelength above 500 nm increases significantly (absorb more orange and red light) as the illumination time increases, which is agree with the color change from yellow to dark [31]. The color change suggests suitable modification in crystal structure and electronic structure which should be related to the hydrogen adsorbed on the ZIS surface during hydrogen evolution reaction [32].

The remarkably enhanced visible light absorption of the UV–vis light treated samples are reasoned to result from the narrowed band gap

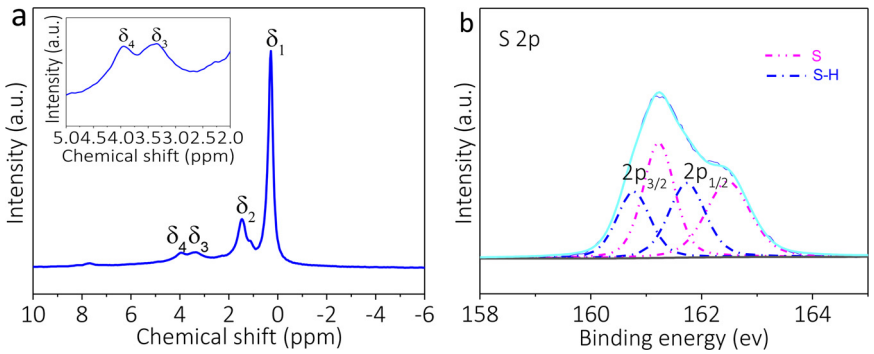

Fig. 2. (a) H^1 solid-state NMR spectrum of the H_xZIS-6 h nanosheets. δ_3 and δ_4 are the signals for S—H bonds; δ_1 and δ_2 are the signals for adsorbed water molecules. (b) XPS spectra of S 2p of H_xZIS-6 h.

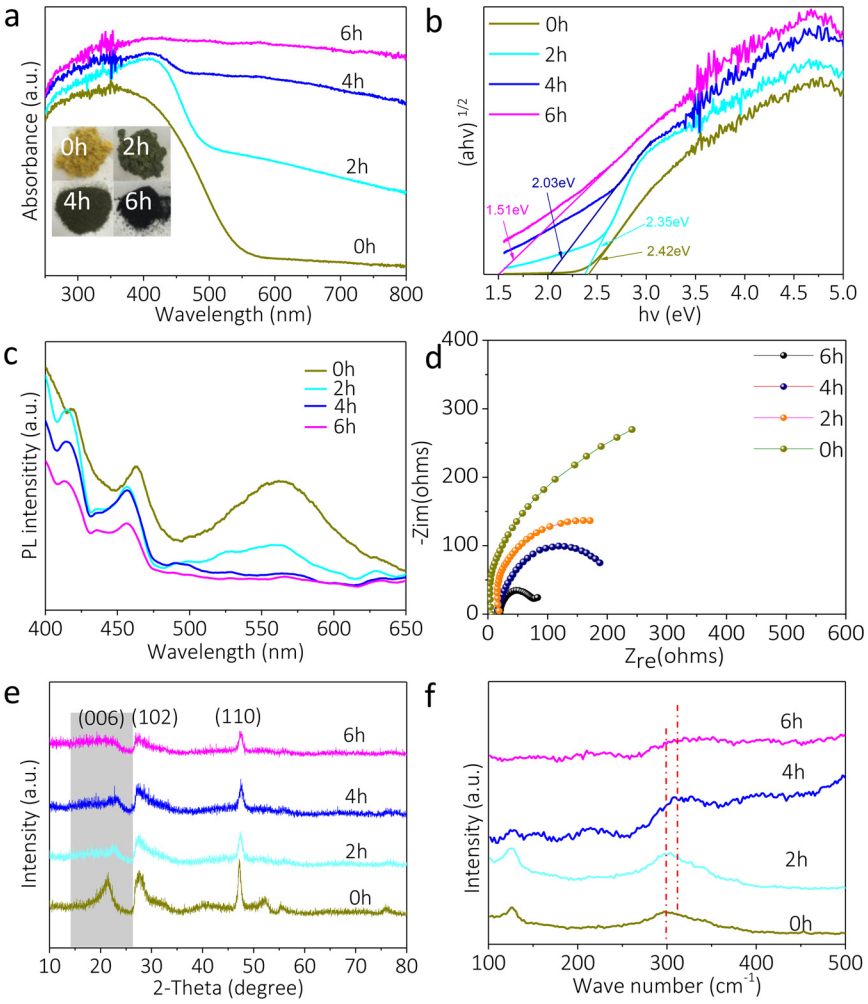

Fig. 3. (a) UV–vis DRS spectra and photographs (inset in a), (b) Tauc plots, (c) Photoluminescence (PL) spectra, (d) Electrochemical impedance spectra, (e) X-ray diffraction (XRD) pattern, (f) Raman spectra of ZIS nanosheets, H_xZIS-2 h, H_xZIS-4 h and H_xZIS-6 h. The excitation source is 350 nm. (For interpretation of the references to colour in the text, the reader is referred to the web version of this article.)

through these treatments (Fig. 3b). The band gap of a semiconductor can be deduced from the equation below:

$$\alpha(h\nu) = A(h\nu - Eg)^{n/2} \quad (1)$$

where α, $h\nu$, Eg, and A are the absorption coefficient, photon energy, band gap, and a constant, respectively. n in this equation depends on the characteristics of the transition in a semiconductor. For H_xZIS, its value is 1 for its direct transition [33]. The Tauc plots of H_xZIS-2 h, H_xZIS-4 h and H_xZIS-6 h are shown in Fig. 3b, which were calculated based on the results of UV–vis DRS. The semiconductor band gap is usually governed by the linear Tauc region, which is just above the optical absorption edge [34]. The specific band gap energies of H_xZIS-2 h, H_xZIS-4 h and H_xZIS-6 h were 2.35, 2.03 and 1.51 eV, respectively. Such a decrease in their band gap energies was in correspondence with the absorption edge result in UV–vis DRS. Obviously, the introduction of proton can make ZIS more effective utilization of solar energy [35].

The steady-state PL spectra in Fig. 3c shows obvious PL quenching of H_xZIS, and H_xZIS-6 h nanosheets showed the lowest PL peak of all the samples. It is commonly known that the PL result represents the recombination rate of free electrons and holes. The stronger PL intensity, the greater is the recombination probability of photogenerated carriers [36]. Accordingly, it is reasonable to conclude that proton in the ZIS nanosheets generated through the facile UV–vis light induced hydrogenation strategy could increase the efficiency of the charge transfer process, resulting in the enhanced charge carrier separate efficiency.

As we all know, the doped hydrogen has a strong impact on the electronic structure of materials by supply additional electrons, and it is very intriguing for us to investigate the impact of hydrogen incorporation on the electrical transport properties of H_xZIS. From the electrochemical impedance spectroscopy (EIS) spectra (Fig. 3d), H_xZIS nanosheets showed a smaller radius than ZIS nanosheets, while ZIS nanosheets with 6 h illumination showed the smallest radius, indicative of fast interfacial charge transfer property in H_xZIS-6 h and the transportation resistance of charge carries along the same layer surface is small [37]. Taken together, all these results conceivably reflect the outstanding advantages of the general UV–vis light induced hydrogenation strategy in ZIS.

In order to investigate the structural changes of the ZIS through the proposed UV–vis light induced hydrogenation strategy, the XRD techniques were performed. The XRD patterns provide direct structural information of the as-obtained H_xZIS. The pristine sample has the typical XRD features of ZIS structure: the typical XRD peaks of hexagonal ZIS at 21.6°, 27.7°, 30.4°, 39.8°, 47.2°, 52.4°, and 55.6°, corresponding to the {006}, {102}, {104}, {108}, {110}, {116}, and {022} lattice planes (JCPDS-03-065-2023), respectively (Fig. 3e) [38,39]. While, there is a shift (at theta ≈ 20°) in the diffraction peaks between pristine ZIS and the H_xZIS samples (Fig. S6). However, diffraction peaks gradually disappear accompanied with the emergence of new peaks in the H_xZIS samples around theta ≈ 20° while other peaks remain the same position with the elongation of illumination time. These new peaks can

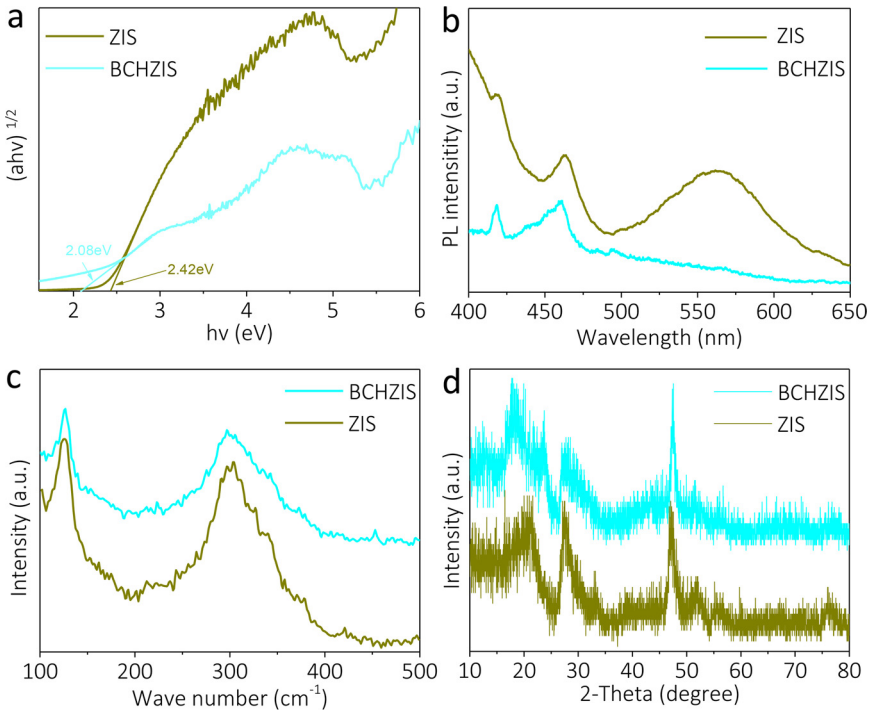

Fig. 4. a) Tauc plots b) Photoluminescence (PL) spectra, c) Raman spectra (d) X-ray diffraction (XRD) pattern of pristine ZIS nanosheets and BCHZIS nanosheets.

be indexed as atom dislocation, indicating the successful hydrogen doping of ZIS [40]. The XRD pattern with weak peaks indicates the weak crystallinity of the H_xZIS nanosheets.

Further insight into the structure of the H_xZIS nanosheets was garnered from their Raman spectrum. As shown in Fig. 3f, the Raman spectra of the ZIS is characterized by two Raman bands around 121 and 300 cm^{-1}, in line with previous report [41]. The strongest peak at 121 cm^{-1} demonstrates the featured layered structure of H_xZIS, and the other peak at 300 cm^{-1} could be assigned to the transverse optical mode (TO_2) of H_xZIS. The possible reason for the broadening of the Raman bands at 300 cm^{-1} in H_xZIS samples, should be the doping effects [42]. The observed red-shift Raman modes at 300 cm^{-1} with elongation illumination time reflect the lattice expansion of the nanosheets, which indicates the accommodation of a large amount of H^+ ions in the ZIS nanostructure [32]. This also means the successful incorporation of proton into the crystal lattice of ZIS, which is in good agreement with XRD measurement.

Furthermore, the structural changes of the H_xZIS through the proposed UV–vis light induced hydrogenation strategy were characterized by scanning and transmission electron microscopy (SEM and TEM) techniques. The SEM image shows that the sample still possessed large-scale 2D sheet-like structures (Fig. S7). From the overview transmission electron microscope (TEM) image of H_xZIS-6 h, the image of nanosheets assemblies (Fig. S8a) confirms the wrinkled thin-layer morphology of the product. The high-resolution TEM (HRTEM) image shows a desultory crystal phase of H_xZIS-6 h (Fig. S8b). Fig. S8c shows the enlarged HRTEM image of H_xZIS-6 h that displays distinct lattice fringes (0.32 nm). Fig. S8d shows the elemental mapping for zinc, indium and sulfur. Their distributions have a perfect spatial correspondence and are uniform throughout the sheet. The corresponding high-resolution TEM (HRTEM) image and fast Fourier transform (FFT) pattern (inset Fig. S8b) further confirm that the H_xZIS-6 h nanosheets don't possess an ordered structure. To probe the composition and spatial distribution of the constituent elements, we also carried out energy-dispersive X-ray (EDX) spectroscopy under scanning transmission electron microscopy (STEM) (Fig. S9).

To further confirm the composition, the valence state of the H_xZIS is characterized by XPS measurement, as shown in Fig. S10. The full scan spectrum indicates the presence of the Zn 2p, In 3d, and S 2p peaks in the sample (Fig. S10a). In addition, a weak peak located at 283.4 eV may be attributed to adventitious carbon derived from the atmospheric CO_2 on the sample surface. The oxygen peak at a binding energy of 531.61 eV originates from H_2O absorbed on the sample surface [43]. The Zn 2p core (Fig. S10b) splits into 2p 3/2 (1021.54 eV) and 2p 1/2 (1044.59 eV) peaks, which are consistent with the values for Zn^{2+}. In 3d core shows two peaks at 444.46 eV (3d 5/2) and 452.19 eV (3d 3/2) (Fig. S10c), corresponding to In^{3+}. The S 2p 1/2 peak at 161.24 eV is ascribed to S coordinated to Zn and In in H_xZIS (Fig. S10d) [44]. All of these results indicate that the chemical states of the sample are Zn^{2+}, In^{3+}, and S^{2-}. More importantly, from the chemical states of S 2p (Fig. S10d), there are two types of sulfur in the illuminated nanosheets corresponding to pristine and hydrogenated samples.

3.3. Characterization of BCHZIS nanosheets (appropriate amounts of adsorbed H)

The above research results show that the bandgap of H_xZIS decreases with the increases of illumination time and the photocatalytic hydrogen evolution rate begins to decrease after 4 h illumination. Such a decrease in the activity of samples with prolonged illumination time is likely due to the excessive amounts of doped H, which excessively narrow the band gap of the ZIS nanosheets and reduce the amounts of excited electrons [45]. In order to maintain the highest activity of the H_xZIS, that requires another step: turn off the UV–vis light and stirring for 12 h under dark to release some of adsorbed hydrogen (BCHZIS nanosheets). The doped H can be deintercalated with vigorous stirring, and the color changed from dark to cyan with the elongation of stirring time, which can be directly proofed by the phenomenon that a small amount of H_2 evolution during stirring.

The Tauc plots of BCHZIS show that the band gap energy of BCHZIS is 2.08 eV, which is beneficial for visible light absorption (Fig. 4a). The steady-state PL spectra of BCHZIS nanosheets have a much lower PL peak (Fig. 4b), this indicates that the recombination rate of free electrons and holes in BCHZIS is very low. Obviously, the remained proton

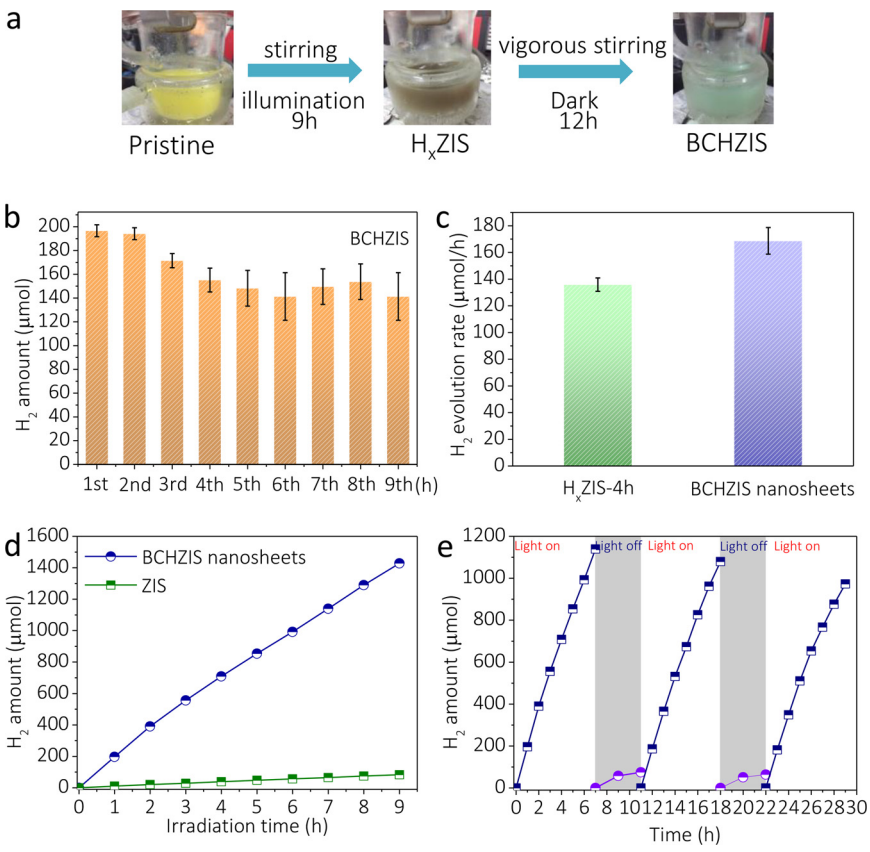

Fig. 5. (a) An illustration of hydrogenation process to understand the relationship between H_xZIS and BCHZIS. (b) H_2 production rate over BCHZIS at each hour of the HER. (c) Average photocatalytic H_2 evolution rate over H_xZIS-4 h and BCHZIS. (d) Photocatalytic hydrogen evolution amount of BCHZIS and ZIS. (e) Photocatalytic H_2 evolution amount with light on and light off (stirring speed, light on: 500 r/min, light off: 1000 r/min). All experiments were carried out in 80 mL of 0.35 M Na_2S and 0.25 M Na_2SO_3 aqueous solution. Light source, 300 W Xe Lamp.

in ZIS can keep it utilize solar energy more efficiently. Then, XRD patterns and Raman spectrum were performed to investigate the structural information. The peaks of BCHZIS at 121 cm^{-1} and 300 cm^{-1} in Raman spectrum are in line with ZIS (Fig. 4c), and the (006) peak in the XRD pattern becomes shaper and stronger with BCHZIS (Fig. 4d), suggesting the increased crystallinity. This phenomenon can be explained by the possibility that the interdomain conductivity was modulated by manipulating the 2D electron conjugation, which was related to the degree of disorder [46]. So, efficient HER activity was achieved for the hydrogen-incorporated ZIS nanosheets with a moderate degree of disorder, proving the validity of the combined structural and electronic regulations for improving the photocatalytic performance.

3.4. Photocatalytic hydrogen evolution of BCHZIS nanosheets

The photocatalytic activities of the UV–vis light treated samples were then investigated by measuring the amounts of hydrogen production from water photo-reduction under a full-spectrum simulator irradiation. The amount of catalyst used was 80 mg in all photocatalytic experiments. Fig. 5a displays an illustration of hydrogenation process to show the relationship between H_xZIS and BCHZIS. Fig. 5b displays H_2 production rate over BCHZIS at each hour of the HER. Fig. 5c clearly illustrates that BCHZIS nanosheets have the average hydrogen evolution rate of 172 μmol/h from 0.35 M Na_2S and 0.25 M Na_2SO_3 aqueous solution. The augmented photocatalytic activity of BCHZIS nanosheets (Fig. 5d) can be attributed to H incorporation that lowers charge-transfer resistance and shortens the diffusion pathway of charge carriers, thus favoring the fast and efficient separation of photogenerated charge carriers [47]. Aside from the higher activity, we also investigated its photocatalytic durability (Fig. 5e). The BCHZIS catalyst was continuously cycled for a total of 3 days under UV–vis light irradiation, meanwhile turn off the light and continue stirring at night to maintain a proper ratio of doped H. Stability and photocatalytic activity of H_xZIS-2 h, H_xZIS-4 h and H_xZIS-6 h were tested as shown in Fig. S11. Furthermore, we have performed the experiment under visible light irradiation (> 420 nm), similar hydrogen evolution trend can be seen from the diagram other than hydrogen amount (Fig. S12). Therefore, by means of hydrogen-incorporation and controllable disorder engineering, an optimized catalyst with an optimal band gap was developed. The apparent quantum efficiency (AQE) for BCHZIS were calculated according to Eq. (2). The calculated AQEs reach 13.2% at 420 nm.

$$\begin{aligned} \mathrm{AQE}(\%) &= \frac{\text{Number of reacted electrons}}{\text{Number of incident photons}} \times 100 \\ &= \frac{\text{Number of evolved } H_2 \text{ molecules} \times 2}{\text{Number of incident photons}} \times 100 \end{aligned} \quad (2)$$

3.5. Proposed reversible hydrogenation mechanism

A gradual yellow to dark was observed under continuous UV–vis light illumination, the following mechanical stirring can bleach the nanosheets back to cyan within hours and the color also can be bleached without stirring after three months (Fig. S13). Spectroscopic analyses show that the nanosheets could be reversibly switched between the colored H_xZIS and the BCHZIS. The coloration is induced by H intercalation and the H could be incorporated into the ZIS network bonding to sulfur ions. The thin-layer morphology of ZIS nanosheets indicates a short ionic diffusion length for surface attached species, which promotes both the surface water decomposition upon UV–vis light irradiation and the proton deintercalation in the bleaching process, therefore, the photochromic property is easy realized. The XRD measurement shows that the peaks in BCHZIS have the similar position compared with pristine ZIS nanosheets, which is due to a small amount of H doped in the ZIS lattice [48]. Our research elucidates that mechanical stirring can bleach the nanosheets back to cyan within hours and the color also can be bleached without stirring after three months, the weak crystallinity of the nanosheets and the wrinkled surface are the main reason for the formation of H_xZIS.

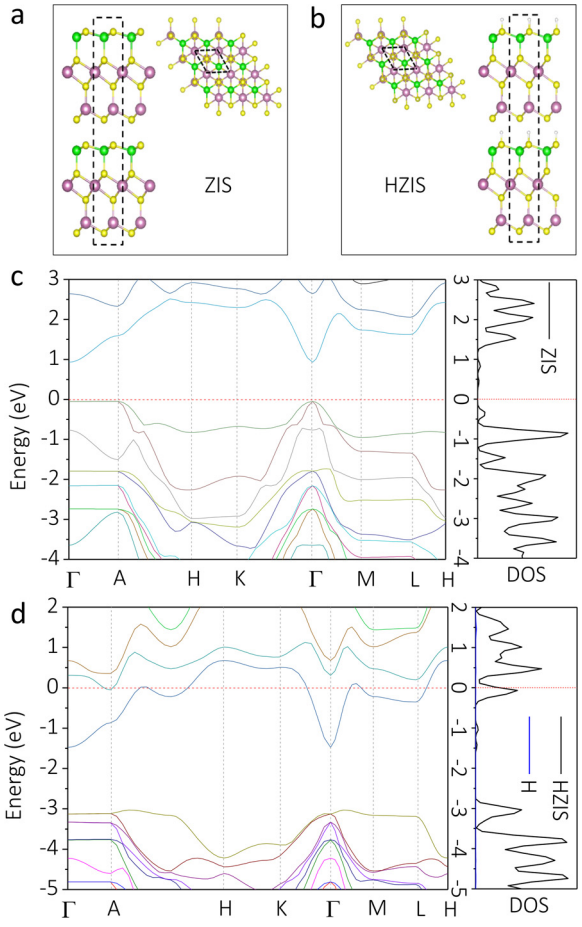

Fig. 6. (a, b) Top and side views of relaxed pristine ZIS systems and H_xZIS systems. (c, d) Electronic densities of states (DOS) of representative pristine ZIS systems, and H_xZIS systems.

In order to reveal the proposed UV–vis light induced hydrogenation process more convincingly, first-principles density functional theory (DFT) calculations have been performed to gain a fundamental understanding of the hydrogenation mechanism. Fig. 6a, b shows the atomic structures of pristine ZIS samples and H_xZIS samples. DOS plots of pristine ZIS samples indicated that pristine ZIS has the semiconductor properties with a certain bandgap in Fig. 6c. However, after H adsorption adsorbed on the surface and insert into inner surface layer. H adsorption changes the overall DOS profile, shifting the Fermi level drastically to reflect complete charge transfer from the H adsorbate. As indicted by DOS plots of H_xZIS samples in Fig. 6d, H_xZIS samples have metallic properties with zero bandgap. Taken together, all these results conceivably reflect the outstanding advantages of the general UV–vis light induced hydrogenation strategy in ZIS nanosheets.

4. Conclusions

In summary, for the first time, in-situ UV–vis light induced hydrogenation method for synthesis of H_xZIS nanosheets was developed. This strategy leads to narrowed bandgap in ZIS nanosheets and improves its solar energy utilization. In alkali, the H_xZIS nanosheets catalyst exhibited efficient and durable activity for the hydrogen evolution reaction, with a more than ten times higher photocatalytic ability. Our DFT calculations manifest that proton doping during photocatalysis plays an important role in PHER. This result represents significant advance in fundamental understanding for the HER catalysis, and we believe that such a facile and general methodology will open up a new path way for the creation of high performance catalyst.

Acknowledgements

This research was supported by the National Natural Science Foundation of China (nos. 51672077, 51378187), China Postdoctoral Science Foundation (Nos. 2018M632956) and Hunan Provincial Natural Science Foundation of China (no. 2017JJ2026). We acknowledge support from Peng Zhang who contribute to the TOC.

Appendix A. Supplementary data

Supplementary material related to this article can be found, in the online version, at doi:https://doi.org/10.1016/j.apcatb.2018.09.062.

References

[1] J. Wu, Z. Zhang, B. Liu, Y. Fang, L. Wang, B. Dong, Solar RRL 2 (2018) 1800039.
[2] N. Lu, Z. Zhang, Y. Wang, B. Liu, L. Guo, L. Wang, J. Huang, K. Liu, B. Dong, Appl. Catal. B: Environ. 233 (2018) 19–25.
[3] Z. Zhang, K. Liu, Y. Bao, B. Dong, Appl. Catal. B: Environ. 203 (2017) 599–606.
[4] Z. Zhang, X. Jiang, B. Liu, L. Guo, N. Lu, L. Wang, J. Huang, K. Liu, B. Dong, Adv. Mater. 30 (2018) 1705221.
[5] Z. Zhang, J. Huang, Y. Fang, M. Zhang, K. Liu, B. Dong, Adv. Mater. 29 (2017) 1606688.
[6] L. Wang, X. Duan, G. Wang, C. Liu, S. Luo, S. Zhang, Y. Zeng, Y. Xu, Y. Liu, X. Duan, Appl. Catal. B: Environ. 186 (2016) 88–96.
[7] Y. Zeng, X. Liu, C. Liu, L. Wang, Y. Xia, S. Zhang, S. Luo, Y. Pei, Appl. Catal. B: Environ. 224 (2018) 1–9.
[8] H. Yu, R. Shi, Y. Zhao, T. Bian, Y. Zhao, C. Zhou, G.I.N. Waterhouse, L. Wu, C. Tung, T. Zhang, Adv. Mater. 29 (2017) 1605148.
[9] R. Shi, Y. Cao, Y. Bao, Y. Zhao, G.I.N. Waterhouse, Z. Fang, L. Wu, C. Tung, Y. Yin, T. Zhang, Adv. Mater. 29 (2017) 1700803.
[10] Y. Zhao, Y. Zhao, G.I.N. Waterhouse, L. Zheng, X. Cao, F. Teng, L. Wu, C. Tung, D. O'Hare, T. Zhang, Adv. Mater. 29 (2017) 1703828.
[11] H. Zhao, X. Ding, B. Zhang, Y. Li, C. Wang, Sci. Bull. 62 (2017) 602–609.
[12] X. Wei, C. Shao, X. Li, N. Lu, K. Wang, Z. Zhang, Y. Liu, Nanoscale 8 (2016) 11034–11043.
[13] C. Tan, Z. Lai, H. Zhang, Adv. Mater. 29 (2017) 1701392.
[14] Z. Zhang, K. Liu, Z. Feng, Y. Bao, B. Dong, Sci. Rep. 6 (2016) 19221.
[15] Z. Zhang, Y. Huang, K. Liu, L. Guo, Q. Yuan, B. Dong, Adv. Mater. 27 (2015) 5906–5914.
[16] P. Niu, L. Yin, Y. Yang, G. Liu, H. Cheng, Adv. Mater. 26 (2014) 8046–8052.
[17] Y. Cao, P. Maitarad, M. Gao, T. Taketsugu, H. Li, T. Yan, L. Shi, D. Zhang, Appl. Catal. B: Environ. 238 (2018) 51–60.
[18] Y. Liu, G. Zhu, J. Gao, M. Hojamberdiev, R. Zhu, X. Wei, Q. Guo, P. Liu, Appl. Catal. B: Environ. 200 (2017) 72–82.
[19] M. Lu, J. Fang, L. Han, K. Faungnawakijc, H. Li, S. Cai, L. Shi, H. Jiang, D. Zhang, Nanoscale 10 (2018) 10528–10537.
[20] Y. Xu, C. Zhang, L. Zhang, X. Zhang, H. Yao, J. Shi, Energy Environ. Sci. 9 (2016) 2410–2417.
[21] J. Tian, Y. Leng, Z. Zhao, Y. Xia, Y. Sang, P. Hao, J. Zhan, M. Li, H. Liu, Nano Energy 11 (2015) 419–427.
[22] X. Chen, L. Liu, P.Y. Yu, S.S. Mao, Science 331 (2011) 746–750.
[23] X. Hu, W. Shao, X. Hang, X. Zhang, W. Zhu, Y. Xie, Angew. Chem. 55 (2016) 5733–5738.
[24] Z. Wang, C. Yang, T. Lin, H. Yin, P. Chen, D. Wan, F. Xu, F. Huang, J. Lin, X. Xie, M. Jiang, Adv. Funct. Mater. 23 (2013) 5444–5450.
[25] W. Zhou, W. Li, J. Wang, Y. Qu, Y. Yang, Y. Xie, K. Zhang, L. Wang, H. Fu, D. Zhao, J. Am. Chem. Soc. 136 (2014) 9280–9283.
[26] M. Yang, Y. Xu, W. Lu, K. Zeng, H. Zhu, Q. Xu, G. Ho, Nat. Commun. 8 (2017) 14224.
[27] L. Wei, Y. Chen, Y. Lin, H. Wu, R. Yuan, Z. Li, Appl. Catal. B: Environ. 144 (2014) 521–527.
[28] J. He, L. Chen, Z. Yi, D. Ding, C. Au, S. Yin, Catal. Commun. 99 (2017) 79–82.
[29] B. Wang, S. He, W. Feng, L. Zhang, X. Huang, K. Wang, S. Zhang, P. Liu, Appl. Catal. B: Environ. 236 (2018) 233–239.
[30] Z. Lei, W. You, M. Liu, G. Zhou, T. Takata, M. Hara, K. Domen, C. Li, Chem. Commun. 17 (2003) 2142–2143.
[31] V. Lau, D. Klose, H. Kasap, F. Podjaski, M. Pignié, E. Reisner, G. Jeschke, B. Lotsch, Angew. Chem. 56 (2017) 510–514.
[32] J. Wei, X. Jiao, T. Wang, D. Chen, J. Mater. Chem. C 3 (2015) 7597–7603.
[33] T. Xiao, Z. Tang, Y. Yang, L. Tang, Y. Zhou, Z. Zou, Appl. Catal. B: Environ. 220 (2018) 417–428.
[34] C. Wang, X. Zhang, X. Song, W. Wang, H. Yu, ACS Appl. Mater. Interfaces 8 (2016) 5320–5326.
[35] H. Fang, X. Zhang, J. Wu, N. Li, Y. Zheng, X. Tao, Appl. Catal. B: Environ. 225 (2018) 397–405.
[36] G. Gong, Y. Liu, B. Mao, L. Tan, Y. Yang, W. Shi, Appl. Catal. B: Environ. 216 (2017) 11–19.
[37] C. Lin, X. Zhu, J. Feng, C. Wu, S. Hu, J. Peng, Y. Guo, L. Peng, J. Zhao, J. Huang, J. Yang, Y. Xie, J. Am. Chem. Soc. 135 (2013) 5144–5151.
[38] Y. Chen, S. Hu, W. Liu, X. Chen, L. Wu, X. Wang, P. Liu, Z. Li, Dalton Trans. 40

(2011) 2607–2613.
[39] Y. Chen, R. Huang, D. Chen, Y. Wang, W. Liu, X. Li, Z. Li, ACS Appl. Mater. Interfaces 4 (2012) 2273–2279.
[40] C. Wu, F. Feng, J. Feng, J. Dai, L. Peng, J. Zhao, J. Yang, C. Si, Z. Wu, Y. Xie, J. Am. Chem. Soc. 133 (2011) 13798–13801.
[41] S. Shen, L. Zhao, X. Guan, L. Guo, J. Phys. Chem. Solid 73 (2012) 79–83.
[42] C. Bi, L. Pan, M. Xu, J. Yin, Z. Guo, L. Qin, H. Zhu, J.Q. Xiao, Chem. Phys. Lett. 481 (2009) 220–223.
[43] Y. Yuan, J. Tu, Z. Ye, D. Chen, B. Hu, Y. Huang, T. Chen, D. Cao, Z. Yu, Z. Zou, Appl. Catal. B: Environ. 188 (2016) 13–22.
[44] Z. Guan, Z. Xu, Q. Li, P. Wang, G. Li, J. Yang, Appl. Catal. B: Environ. 227 (2018) 512–518.
[45] C. Liu, L. Wang, Y. Tang, S. Luo, Y. Liu, S. Zhang, Y. Zeng, Y. Xu, Appl. Catal. B: Environ. 164 (2015) 1–9.
[46] J. Xie, H. Zhang, S. Li, R. Wang, X. Sun, M. Zhou, J. Zhou, X. Lou, Y. Xie, Adv. Mater. 25 (2013) 5807–5813.
[47] Y. Wang, Y. Zhang, Z. Liu, C. Xie, S. Feng, D. Liu, M. Shao, S. Wang, Angew. Chem. 56 (2017) 5867–5871.
[48] Y. Filinchuk, N.A. Tumanov, V. Ban, H. Ji, J. Wei, M.W. Swift, A.H. Nevidomskyy, D. Natelson, J. Am. Chem. Soc. 136 (2014) 8100–8109.